JOURNAL OF PROPULSION AND POWER
Vol. 16, No. 6, November–December 2000

Mass Spectral Measurements in the Plume of an SPT-100 Hall Thruster

Lyon B. King* and Alec D. Gallimore†
University of Michigan, Ann Arbor, Michigan 48105

Knowledge of the ion species emitted by the SPT-100 Hall thruster provides considerable insight to basic thruster performance. To gain detailed information concerning the composition of the plume plasma, a unique molecular beam mass spectrometer was constructed to interrogate the exhaust plume. An investigation using this technique yielded both the ionization fraction of the xenon propellant and a qualitative analysis of the minority plasma species attributed to ground-test facility interactions. The plasma was found to consist of 89% Xe^{+}, 11% Xe^{2+}, and 0.2% Xe^{3+}. The existence of parasitic facility gasses including nitrogen, oxygen, and water vapor was documented, as well as trace carbon ions caused by sputtering of graphite surfaces in proximity of the thruster.

Nomenclature

D_{coll}	=	molecular beam mass spectrometer (MBMS) collimator diameter, mm
D_s	=	MBMS inlet skimmer diameter, mm
d_{gate}	=	gate electrode length, m
E_{coll}	=	energy of collision, J or eV
E_i	=	ion energy, J or eV
E_p	=	most probable ion energy, J or eV
E_{-1}	=	ion energy where distribution drops by a factor of e^{-1} from maximum, J or eV
e	=	elementary charge, C
$F(E_I)$	=	ion energy distribution, J^{-1}
$f(E/q)$	=	ion voltage distribution, V^{-1}
$f(u_I)$	=	ion velocity distribution, $(m/s)^{-1}$
G_{CEM}	=	electron multiplier gain
I	=	ion current, A
M_i	=	ion atomic mass number, atomic mass unit (amu)
m_i	=	ion mass, kg
m_p	=	atomic mass constant, kg
$m_{1,2}$	=	mass of species 1, 2, kg
n_i	=	ion density, m^{-3}
q_i	=	integer ion charge state
r	=	radial distance from thruster, m
s	=	gate interelectrode spacing, m
T_{eV}	=	ion temperature, eV
T_i	=	ion temperature, K
t	=	time, s
t_{gate}	=	gate open duration, s
t_{tof}	=	ion time of flight, s
u_d	=	bulk ion drift velocity, m/s
u_i	=	ion velocity, m/s
V_i	=	voltage, V
V_p	=	most probable ion voltage, V
V_{-1}	=	ion voltage where distribution drops by a factor of e^{-1} from maximum, V
α_n	=	voltage-dependent fraction of Xe^{n+}
θ	=	angle, deg
Φ_n	=	global flow fraction of Xe^{n+}

Received 23 October 1998; revision received 15 November 1999; accepted for publication 20 December 1999.

*Research Associate, Plasmadynamics and Electric Propulsion Laboratory, Department of Aerospace Engineering; currently **(job title)**, National Institutes of Standards and Technology, Time and Frequency Division 847, 325 Broadway, Boulder, CO 80303; Lyon.King@boulder.nist.gov.Member AIAA.

†Associate Professor, Plasmadynamics and Electric Propulsion Laboratory, Department of Aerospace Engineering; 3037 FXB Building; Alec.Gallimore@umich.edu. Associate Fellow AIAA.

I. Introduction

In situ plasma probes constitute a simple method through which detailed plasma properties can be evaluated. However, these probes provide no insight to plasma species (charge-state and mass) composition. Indeed, the retarding potential analyzer (RPA) technique of measuring the ion energy distribution function is not merely insensitive to flow species, rather its interpretation is only valid for a single species. Although RPAs enjoy widespread use in plasma diagnostics, it must be recognized that, in a multiple-species flow, differentiation of the $I(V)$ vs V data does not produce a function directly proportional to the energy distribution as widely accepted, instead

$$\frac{\mathrm{d}I}{\mathrm{d}V} \propto \frac{q_i^2}{m_i} f\left(\frac{E_i}{q_i}\right) \tag{1}$$

The nontrivial relationship between the RPA data and the ion energy places a limitation on the rigor with which the resultant quantities can be applied.[1]

Further complicating the understanding of RPA data has been the extensive documentation of a high-energy tail of ions with seemingly impossible accelerating voltages much greater than that applied between the anode and cathode of the Hall thruster.[2–6] This tail has been the subject of much controversy and confusion of late; postulates to explain its existence include plasma instability-driven turbulence within the thruster discharge as well as recombinative or charge-changing collisions within the exhaust plume. Exploration of these hypotheses requires species-dependent analysis of the plasma energy.

As a means of quantifying the plasma species constitution and obtaining a verification of the puzzling ion-energy distribution, Manzella utilized spectroscopic techniques to interrogate the Hall-thruster plasma.[7] In these studies, emission spectroscopy was used to measure the xenon ionization fractions and plasma temperature.[7] The emission study determined that the fraction of Xe^{+} was 89% of the total flow while Xe^{2+} comprised 11.9%, with a common distribution temperature of 0.7 eV. However, the author acknowledged that the Boltzmann equilibrium model used to derive these values from the data was possibly not well suited to the Hall-thruster plasma. Although the correct model was identified as a collisional-radiative equilibrium (CRE) model, no such model was developed for several reasons attributed to the complicated atomic energy structure of xenon coupled with a lack of experimental data regarding various excitation rates. The spectroscopically measured distribution

energy spread of 0.7 eV seemed to disagree with the RPA data, which demonstrated a width on the order of 100 V.

The state of research preceding the study reported here reflected conflicting and uncertain information regarding the ionic composition and energy within the Hall-thruster plume: the only species analysis performed required the use of a complex model to achieve estimates of propellant ionization fraction, whereas the two existing measurements of ion energy distribution seemed to be inconsistent. It was apparent that a technique was required 1) to provide a direct measure of the propellant ionization fraction independent of a model regarding the plasma equilibrium state and 2) to measure directly the energy distribution function of each species using a method that is sensitive to ionic charge and mass. Based on this need, the construction of a custom-built molecular beam mass spectrometer (MBMS) for Hall-thruster plume studies was initiated.

II. Description of Apparatus

The MBMS system used a set of orifice skimmers to admit a beam of plume ions from the main vacuum chamber into an array of differentially pumped subchambers. The instrument is shown in Fig. 1. The subchambers were maintained at high vacuum to minimize and effectively eliminate collisions involving ions within the beam. A sampling skimmer orifice was mounted on the upstream end of the MBMS; this orifice skimmed off a small-diameter ion beam into the first subchamber. This beam was then collimated by a second orifice at the downstream end of the first subchamber. The collimated beam then passed through the entrance slit of a 45-deg electrostatic energy analyzer. This analyzer employed a constant electric field such that only ions with a preselected voltage (energy per charge, since $V_i = E_i/q_e$) have a trajectory that permits them to traverse the exit slit and impinge on a ceramic channel electron multiplier (CEM). By recording the output current of the CEM as a function of the electric field strength within the 45-deg analyzer, the ion energy distribution function was evaluated. A more detailed discussion of the energy analyzer can be found in Refs. 1 and 8.

Mass analysis was obtained by using an electrostatic beam gate to chop the ion beam immediately downstream of the inlet skimmer and to record the time required for an ion to pass from the gate to the detector: Because the 45-deg analyzer admits only ions with a preselected value of $m_i u_i^2/2q$ to the CEM, ions of different mass but the same energy per charge will have different velocities and, hence, will arrive at the detector at different times. The configuration of the instrument was based on that of Pollard.[9] The beam gate consists of two planar electrodes of length d_{gate} placed on opposing sides of the ion beam at distance s apart. A large voltage difference (around 1.5 kV) is applied between the plates creating a strong electric field perpendicular to the ion beam line. This field deflects all ions such that their trajectories intersect the chamber wall. At time $t = 0$, this electric field is removed for a period of time lasting t_{gate}, opening the gate and admitting a pulse of ions to the field-free drift region of length d_{tof}. Each ion species arrives at the CEM a time t_{tof} after the start of the gate pulse according to

$$M_i/q_i = \left(d_{\text{tof}}^2/t_{\text{tof}}^2\right)(2eV_i/m_p) \tag{2}$$

In Eq. (2) the drift length d_{tof} can be easily measured, the ion voltage V_i is determined by the 45-deg analyzer, and m_p is the atomic mass constant in kilograms. Thus, by measuring the flight time t_{tof}, the ion mass per charge is easily obtained. A high-speed transimpedance preamplifer was used to convert the CEM output current to voltage; this voltage was then postamplified using a fast operational amplifier circuit. Combining the gain of the CEM with the amplifier circuitry yields an overall system gain of 2.5×10^{14} V/A for the ion beam current. A much more detailed description of this apparatus and the defining design constraints may be found in Ref. 1. A summary of the MBMS physical parameters is presented in Table 1.

III. Experimental Setup

The experiments reported in this paper were performed in a 6-m-diam × 9-m-long stainless-steel vacuum chamber at the University of Michigan. A detailed description of this facility may be found in Ref. 10. Background chamber pressure was maintained at less than 4 mPa when the Hall thruster was operating on approximately 5 mg/s of xenon. The thruster utilized in this research was a flight-model stationary plasma thruster (SPT) 100 manufactured by the Fakel Design Bureau. The SPT-100 was operated at nominal conditions of 300 V at 4.5-A discharge controlled through a power-processing unit manufactured by Space Systems/Loral. The total propellant flow rate was 56 standard cubic-centimeters-per-minute with 7% of the total flow diverted through the hollow cathode. The SPT-100 was mounted to a rotary table such that the rotation axis coincided with the center of the exit plane of the thruster. Therefore, by the rotation of the thruster relative to the fixed MBMS skimmer inlet, the plasma plume could be sampled as a function of angular position at a fixed radial distance r from the exit plane. This setup is shown schematically in Fig. 2. The circuitry used to obtain the time-of-flight (TOF) spectra and convert the data into mass-per-charge spectra is shown in Fig. 3.

The centerline (thrust axis) of the thruster was denoted as 0 deg, with positive theta values representing points in the cathode half-plane of rotation (the angular position shown in Fig. 2 represents $\theta = +90$ deg). The angular alignment of the thruster and MBMS was achieved using a laboratory laser to establish the MBMS beam line. The laser beam line was used to verify the angular orientation of the 45-deg electrostatic analyzer to within 0.5 deg; similarly, the thruster was rotated such that the laser beam line was precisely aligned with the center of the exit plane of the thruster, as shown in Fig. 2, establishing the 90-deg position of the SPT-100 to better than 0.5 deg. Because the relative uncertainty in angular position of

Table 1 Physical parameters of MBMS time-of-flight components

Parameter	Value
d_{tof}	2.35 m
d_{gate}	1.3 cm
s	1 cm
D_s	5 mm
D_{coll}	3 mm

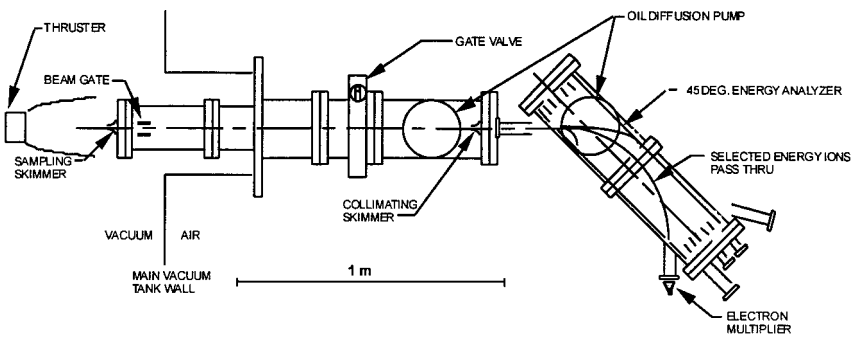

Fig. 1 Schematic of overall configuration of MBMS apparatus showing orientation to main vacuum chamber, thruster mount, and scale size.

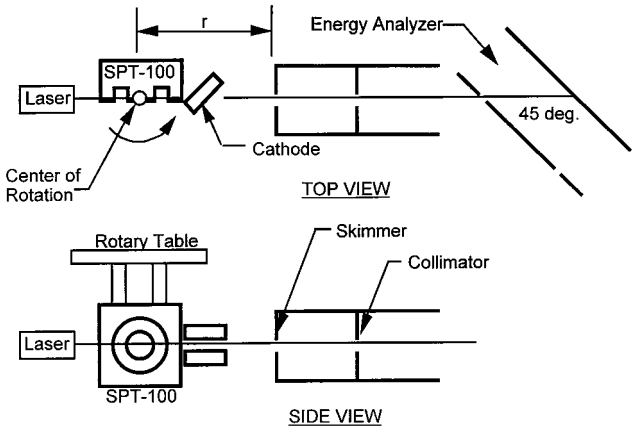

Fig. 2 Experimental setup showing rotary thruster mount and laser alignment of beam.

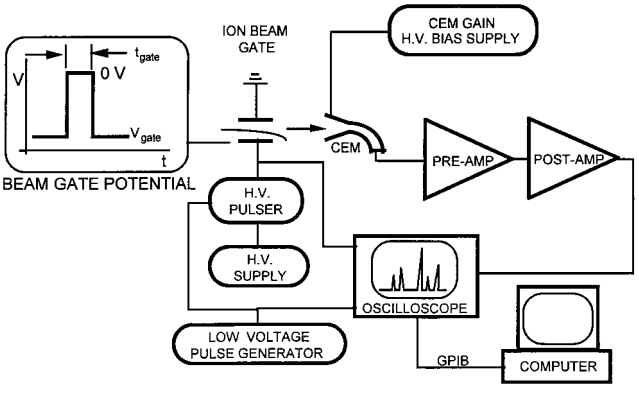

Fig. 3 Electrical schematic of controlling electronics and data system for TOF spectrometer.

the rotary table was 0.1 deg, the uncertainty in position for all data points is ±0.5 deg due to initial alignment uncertainty.

The inlet of the MBMS was grounded, while the plasma maintained a potential that was somewhat higher than ground. To account for the instrument-induced energy addition as plume ions fell from local plasma potential to ground potential, a cylindrical langmuir probe was placed immediately upstream of the skimmer face, outside of the sheath formed on the skimmer. The plasma was approximated as a homogeneous, unmagnetized Maxwellian, and standard collisionless probe theory was used to deduce the plasma potential from the current–voltage characteristic.[11] The deduced value of plasma potential was approximately 8 V higher than MBMS ground. This artificial energy increase was subtracted from the data through postprocessing.

IV. Results

As a demonstration of the data interpretation principles for the TOF system, Fig. 4 shows a typical TOF spectrum obtained for a 45-deg analyzer ion pass voltage of 280 V at a position of 0.5-m radius and 5 deg off axis. The potential difference across the gate electrodes was maintained at 1.5 kV nominally. At time $t = 0$, this potential difference was removed with a rise time of 40 ns, opening the ion gate for a time $t_{gate} = 5\ \mu$s. This high-voltage transient induced switching noise into the facility ground plane, which appeared as a noise burst in the CEM amplifier circuitry; this noise rapidly decayed after the pulse returning to a zero-current baseline. The transient current peaks appearing in the CEM output signal represent the arrival of different ion species at the detector. For example, from Eq. (2) for 280-V ions, singly ionized xenon with $M_i/q_i = 131$ atomic mass unit (amu) would take 120 μs to travel the 2.35-m path and arrive at the detector; this species is seen as the dominant peak. Doubly ionized xenon has $M_i/q_i = 65.5$ amu and, therefore, corresponds to the peak seen at $t = 85\ \mu$s. The conversion between time

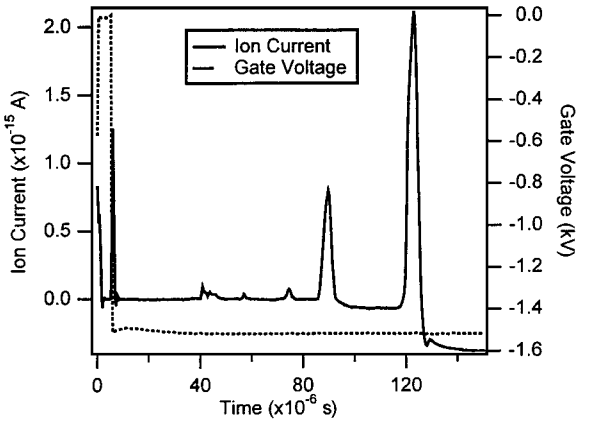

Fig. 4 Typical TOF spectra for 280-V ions at 0.5 m radius from the SPT-100 for the point 5 deg off thruster axis: - - - -, beam gate potential and corresponds to the right axis and ——, ion current measured by the CEM, which is scaled on the left axis.

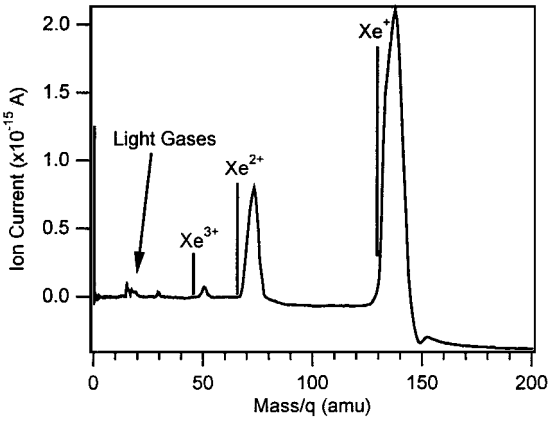

Fig. 5 Typical mass spectrum for 280-V ions derived from data of Fig. 4.

and mass-per-charge can be performed yielding the mass spectrum shown in Fig. 5. In Fig. 5 the baseline offset displayed after an intense current peak was due to preamplifier undershoot.

This mass spectra shows the first three ionization states of the propellant, xenon, along with a small population of light gasses with M_i/q less than 30 amu. Many of the characteristics illustrated in this spectra are typical of all data points. As a result of the quadratic conversion between arrival time and species mass, the heavier mass peaks, although equal width in time, are wider in terms of amu than the lighter masses. Although the peak widths are on the order of 10 amu, this width does not impose any difficulty with mass identification of propellant ions: The leading (left) edge of the mass peak marks the arrival time of the species and, therefore, the species mass, whereas the peak width represents the duration of the gate open time.

In an attempt to identify better the light gasses evidenced in Fig. 5, the gate pulse was narrowed, and the oscilloscope was configured to obtain better resolution for these minor species. However, the extremely short gate-pulse duration necessary to resolve the light gasses negates any quantitative information that can be obtained from the species peak height. This phenomenon results from the physical length of the gate region. If the gate open time is shorter than the time required for an ion to traverse the gate distance d_{gate}, then the ion mass peak will be attenuated. This principle is fully explained in Ref. 1. Regardless of the ambiguous peak height, though, the species M_i/q can still be accurately observed to provide identification of the plasma components. The resulting minor species spectrum is shown in Fig. 6.

Based on the problems involved with deriving quantitative information for light-gas species, all quantitative analyses were limited to the ionization states of the heavy propellant, xenon. Thus, mass spectra were obtained at the fixed position of 0.5 m, 5 deg, as a

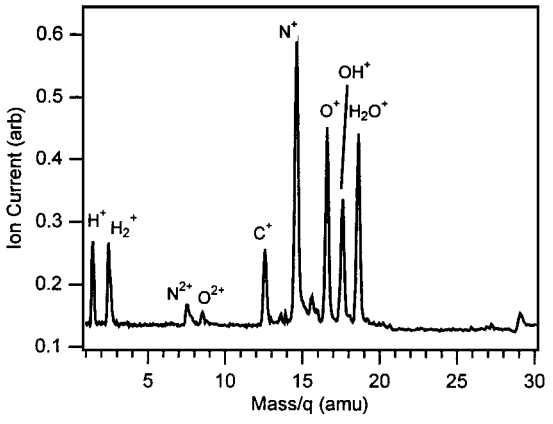

Fig. 6 Minor species identification for 280-V ions at 0.5-m radius from the SPT-100 for the point 5 deg off thruster axis.

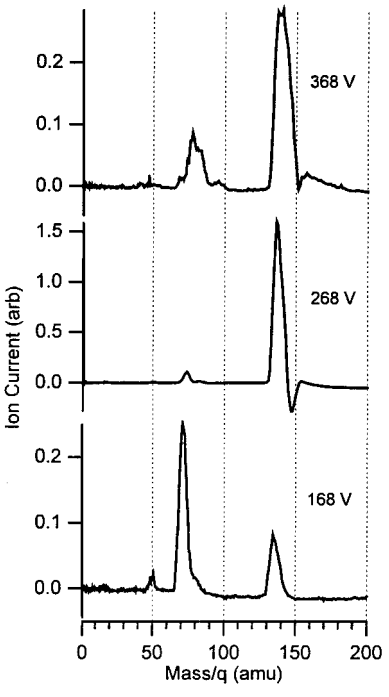

Fig. 7 Mass spectra for evaluation of xenon ionization states for ions with 168-, 268-, and 368-V acceleration in the SPT-100 at 0.5 m radius, 5 deg off thruster axis.

function of ion voltage with the gate-pulse duration sufficient to resolve the ionization states of xenon with full transmission of current peaks. This was accomplished by using the 45-deg analyzer to define the pass voltage and by taking a TOF mass spectrum for only ions with this voltage. To avoid possible confusion, it is emphasized that the thruster operation parameters of 300-V applied discharge at 4.5 A were not changed during testing; the voltages indicated for the TOF spectra correspond to the ion energy/q being analyzed in the MBMS for the fixed thruster discharge. Figure 7 illustrates the mass spectra obtained for ions with voltages of 168, 268, and 368 V at the fixed SPT-100 operating point of 300 V at 4.5 A. In Fig. 7, it is clear that the low-energy ion population is dominated by Xe^{2+} (over 60% of the ions at 168 V are doubly charged), whereas the high-energy ions are mostly Xe^{+}. Note that in Fig. 7 no attempt was made to obtain narrow peaks of high mass resolution; on the contrary, the gate-pulse duration was set excessively long to ensure the full transmission of the ion current pulses such that the peak height indicated a true measure of ion density fraction.

V. Discussion

A. Minor Species Analysis

The spectra obtained for identification of the minor species, shown in Fig. 6, shows results consistent with previous investigations. In an emission spectroscopic study, Manzella documented clear evidence of the ingestion and ionization of background gas from the vacuum facility within the SPT-100 discharge.[7] Because of facility pumping imperfections, a trace amount of parasitic background gas exists within the chamber during testing. This gas consists mainly of atmospheric components, that is, nitrogen and oxygen, with a disproportionate amount of water vapor. The neutral background gas diffuses into the thruster discharge chamber where it is ionized and accelerated back out with the propellant ions. Manzella estimated a quantity of entrained background ions equivalent to 2% of the main propellant flow.[7]

The minority species evaluation reported here supports the finding of ingested facility gasses. Because of the molecular dissociation of the water molecule under electron impact ionization, this species produces peaks at $M_i/q = 18$ (H_2O^+), 17 (OH^+), 2 (H_2^+), and 1 (H^+). The existence of singly ionized carbon in the plume signature arises from facility effects as well. To prevent material damage to the vacuum chamber walls immediately behind the MBMS inlet skimmer because of impacting high-energy ions, these surfaces were extensively coated with low-sputter-yield flexible graphite sheets. Evidence of substantial ablative sputtering of the graphite was apparent as a thin gray film deposited on metallic facility surfaces during posttest inspections and reconfigurations; ingestion of this sputtered graphite is the likely source of the $M_i/q = 12$ signature in the minority spectrum.

B. Propellant Ionization

Analysis of the propellant ionization state was accomplished by recording individual mass spectra for ion voltages ranging from 100 up to 620 V at 20 V increments. Such a data set enabled the ionization fraction of each xenon species to be calculated as a function of ion voltage. The ion species current peaks are related to their respective ion densities through the value of ion charge state: The current output of the CEM for a given ion voltage and charge state is

$$I_i(V_i, q_i) = G_{\mathrm{CEM}} e n_i \sqrt{2 q_i e V_i / m_i} \tag{3}$$

It should be noted that, due to the particle-counting nature of CEM measurements, the measured output current is not directly proportional to q_i as might be accepted.[1] Thus, for a given species, the density and the current are related according to

$$n_i(q_i) \propto I_i(q_i) \Big/ \sqrt{q_i} \tag{4}$$

Defining the number density fraction of Xe^{n+} having energy/$q = V_i$ as $\alpha_n(V_i)$ yields

$$\alpha_n(V_i) = \frac{I(V_i, n) \Big/ \sqrt{n}}{\sum_q I(V_i, q) \Big/ \sqrt{q}} \tag{5}$$

In the analysis of the propellant mass spectra, xenon ions up to $q = 3$ were readily measured, with no conclusive evidence of Xe^{4+} exhibited in the spectra; complicating the search for Xe^{4+} was that the mass per charge of this ion is 32.2 amu, which is very close to the 32 amu attributable to singly ionized O_2 present due to parasitic facility gasses. Therefore, the mass spectra were inconclusive in identifying quadruply ionized xenon. The values of α_n were calculated from an assembly of mass spectra obtained at 20-V intervals of ion voltage recorded over a range from 100 to 620 V (such as those shown in Fig. 7 for ion voltages of 168, 268, and 368 V). From each mass spectrum at a given ion voltage, α_n was computed according to Eq. (5); the results are compiled as Fig. 8, which shows a plot of the number density fraction of the first three ionization states of xenon plotted as a function of ion voltage. Compared with this plot is the total (species independent) ion voltage distribution function from Ref. 8.

Figure 8 indicates that the majority of the plume ions have undergone accelerations through approximately 270 V; of these ions, almost 90% are singly ionized. Although the ion density decreases for voltages less than 270 V, a greater fraction of these low-voltage ions are multiply charged with nearly 100% of the 110-V ions consisting of Xe^{2+}. The number fraction of Xe^{3+} peaks at about 6% of the ions having voltages of 150 V. For voltages greater than the most

Table 2 Comparison between MBMS-measured ionization fractions with values derived from Manzella's[7] study[a]

Species	Φ_n from MBMS[b]	Φ_n from Manzella[7]
Xe^+	0.888	0.89
Xe^{2+}	0.110	0.119
Xe^{3+}	0.002	(not measured)

[a]Optical emission spectroscopy used.
[b]Uncertainty in MBMS values is approximately 5%.

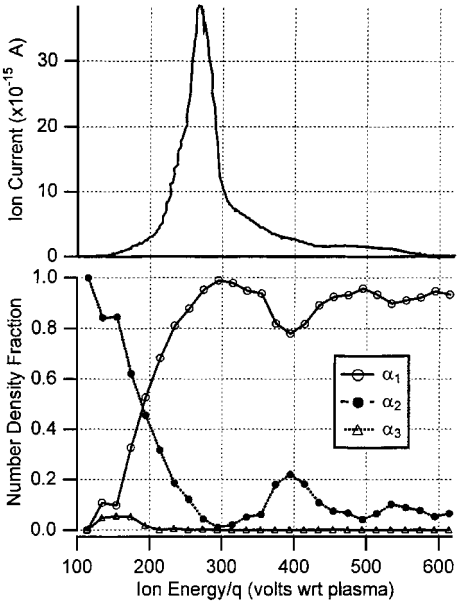

Fig. 8 Number density fractions of the first three ionization states of Xe as a function of ion energy at 0.5 m radius and 5 deg off thrust axis in the SPT-100; top curve shows value of total ion current as a function of ion voltage for comparison of total density.

probable voltage, the fraction of multiply charged ions experiences a slight increase over the composition at 270 V.

The total number density fractions for all ions in the plume can be obtained by integrating the voltage-dependent flow fractions over all voltages. Denoting the overall fraction of ions with charge $q_i = n^+$ as Φ_n, we have

$$\Phi_n = \frac{\int_0^\infty \alpha_n(V) I(V)\,\mathrm{d}V}{\int_0^\infty I(V)\,\mathrm{d}V} \tag{6}$$

The total flow fractions computed from the MBMS data according to Eq. (6) and the data of Fig. 8 are compared with the fractions calculated by Manzella[7] using an optical emission spectroscopic technique at the thruster exit plane; this comparison is shown in Table 2.

The agreement between the two techniques demonstrated in Table 2 is excellent, exhibiting only negligible differences. Additionally, the MBMS system provided the first ever documentation of the existence of Xe^{3+} within the Hall-thruster plume. Note that the MBMS-measured ionization fractions were obtained for the single position of 5 deg off thrust centerline at 0.5 m radius, whereas the emission spectroscopic fractions represent an integration over the entire exit plane region of the thruster. Continued studies of the propellant ionization as a function of spatial position within the plume are indeed warranted.

Further insight into the propellant ionization and acceleration mechanism is possible through analysis of the TOF spectra. As discussed earlier and evidenced by Eq. (1), the existence of multiple ion species presents considerable difficulty in determining the ion energy distribution function using a method insensitive to ion charge state. However, by the compilation of the species current peak heights in the TOF spectra as a function of ion voltage, it is possible to construct true ion-energy distribution functions independently for each ion species in the flow. These data are shown in Fig. 9.

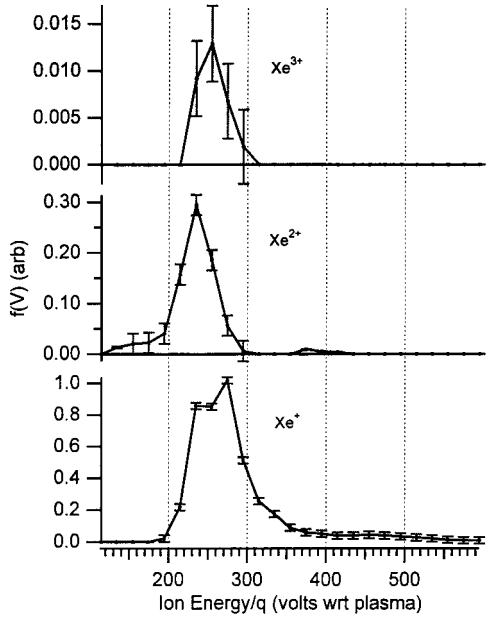

Fig. 9 Ion voltage distribution function for each propellant ionization state in the SPT-100 at 0.5 m radius and 5 deg off thruster axis.

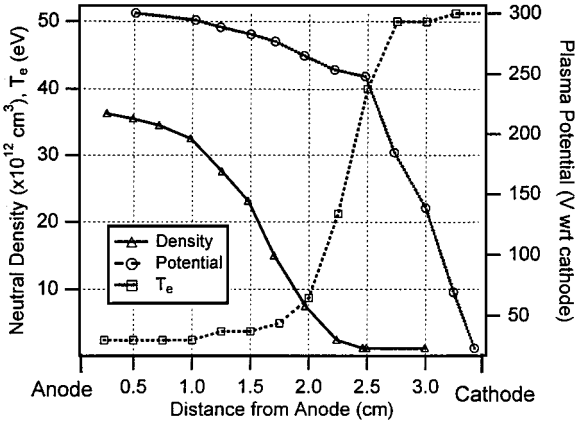

Fig. 10 Results of Baranov model[13] of plasma parameters in Hall-thruster discharge chamber including neutral atom density (left axis), electron temperature (left axis), and plasma potential (right axis).

The species-dependent energy distributions display some subtle, yet remarkable, features. The highest most-probable voltage is displayed by Xe^+, with $V_m = 274$ V, with the peaks in the multiply charged ions at lower voltages. This finding is consistent with the ionization and acceleration processes believed to exist within the thruster discharge chamber as discussed next.

It has been widely documented that the electron temperature within the discharge chamber attains a maximum in the region of highest magnetic field strength, which occurs very near the thruster exit plane.[12,13] Indeed, this behavior was displayed in the model by Baranov[13]; Fig. 10 shows the results of his model in predicting neutral density, electron temperature, and plasma electric potential.

The energy required for the first ionization of neutral xenon is 12.1 eV, whereas the second ionization potential is 21.21 eV (Ref. 14). Therefore, as the neutral atoms travel from the anode toward the exit plane, the initial electron collisions will have sufficient energy for single ionization, but insufficient energy to form a multiply charged ion; formation of the multiply charged ions will occur farther downstream, where the electrons are hotter and, as a result of the distribution of plasma potential, experience less accelerating voltage. The ionization potential of Xe^{3+} is 32.1 eV (Ref. 14). This

would imply that the most-probable voltage of the triply charged ion should be less than that of Xe^{2+}. However, Fig. 9 shows the distribution peak for Xe^{3+} to be 255 V whereas Xe^{2+} exhibits a peak at 235 V. This behavior is contrary to the ionization and acceleration mechanism described earlier. The reason for this anomaly is believed to stem from uncertainty in determining the peak heights corresponding to Xe^{3+} in the TOF spectra compiled in Fig. 9: Because the triply charged xenon ion represented only 0.2% of the total mass flow, the current peaks were extremely small and occasionally difficult to resolve in the TOF spectra. Combined with the 20-V resolution obtained by acquiring TOF spectra in 20-V intervals, this uncertainty could be responsible for a 20-V uncertainty in most-probable voltage location for the $f(V)$ curve.

C. Comments on the High-Energy Tail

As discussed in the Introduction, the existence of a high-energy tail within the measured energy distribution of Hall thrusters has eluded explanation. A detailed discussion of the mechanism responsible for this feature may be found in Ref. 1. A brief account of this phenomenon will be presented here.

The accelerating potential available for propellant ions is fixed by the voltage applied between the anode and the cathode of the Hall thruster, which, for the SPT-100, is 300 V. If the plasma is assumed to consist entirely of $q = 1$ ions, then the existence of ions possesing equivalent acceleration voltages greater than 300 V is indeed physically prohibited. However, the confusion is easily removed through the realization of a collisional multispecies plasma and proper identification of the filtering characteristics of electrostatic analyzers such as RPAs and the 45-deg configuration used in this study.

There exist two different collisional effects capable of producing the anomalous distributions observed in this paper. To understand how the first colisional effect can produce ions with apparent voltages greater than that applied to the discharge, it is important to realize the nature of electrostatic analyzers. As discussed fully in Ref. 1, such techniques do not measure true ion energy, instead they measure the equivalent ion voltage, which is the energy per charge ($V_i = E_i/qe$). Thus, a change in the ion charge state occuring after the initial acceleration can have drastic effects on the measured distribution. Consider, for example, the Xe^{3+} voltage distribution displayed in the top of Fig. 9. As shown in the data, the majority of Xe^{3+} ions experienced an acceleration, or energy per charge, of approximately 250 V. The occurrence of a single-electron charge exchange collision with neutral facility background gas can transform this ion to Xe^{2+} with no change of kinetic energy. Thus, on detection in the MBMS or RPA, this ion will appear as Xe^{2+} with a voltage (energy per charge) of $\frac{3}{2}$ times its original value of 250 V, or 375 V. Examining the distribution of Xe^{2+} from Fig. 9 indeed indicates a small population centered exactly at 375 V. This feature also appears in the bottom of Fig. 8, where the fraction of Xe^{2+} is elevated near 375 V due to the population of this regime by the charge-exchange collisions from the more energetic Xe^{3+}. Further documentation of such high-energy bumps in the distribution can be found in Ref. 15, which include additional convincing evidence of high-energy distributions occurring at two times the acceleration voltage arising from charge exchange transforming an Xe^{2+} into an Xe^{+}.

The second mechanism contributing to the high-energy tail is also apparent in the data presented in this study. This scenario involves energy transfer between ionic species through momentum exchange collisions. Because of the nature of the electrostatic acceleration, a doubly charged ion will achieve twice the kinetic energy of a like-mass singly charged ion when subject to the same voltage. Thus, the Xe^{2+} is traveling at a greater velocity than the Xe^{+} on emission from the thruster. Elastic collisions between these two species, then, will result in the Xe^{+} being speeded up by the overtaking Xe^{2+}, with a corresponding loss of velocity for the Xe^{2+} product. These collisions will result in the growth of a high-energy tail on the Xe^{+} distribution, which must decay to zero at two times the maximum voltage of the Xe^{2+} reactants (about 600 V in this case because the Xe^{2+} reactant distribution decays to zero at 300 V) because this value represents the maximum energy available from the energetic Xe^{2+} collision partner. Similarly, the Xe^{2+} distribution obtains a corresponding low-energy tail decaying to zero at a voltage of one-half the minimum voltage of the Xe^{+} reactant, or approximately 100 V for the conditions reported here. This behavior is strongly suggested by the data shown in Fig. 9, where the Xe^{2+} curve displays the expected low-energy tail in concert with the high-energy counterpart of the Xe^{+} distribution.

D. Ion Temperature

The spectroscopic data of Manzella indicated an ion temperature of 0.7 eV in the xenon plasma of the SPT-100 plume.[7] When compared with the RPA and MBMS-measured ion energy distributions, which have widths on the order of 100 V (see Fig. 8), it is not readily apparent if these two indications of the ion-energy spread are consistent. Indeed, much controversy has surrounded this contradiction in the two methods. Upon proper analysis, however, it will be shown that these two independent measurements of the ion temperature are in excellent agreement.

To define the temperature, this analysis will assume a Maxwellian distribution imposed on a drifting reference frame:

$$f(u_i) = \sqrt{\beta/\pi}\exp\left[-\beta(u_i - u_d)^2\right] \tag{7}$$

where u_d is the mean ion speed and $\beta = m_i/2kT_i$. Note that $u_i = (2E_i/m_i)^{1/2}$; this distribution can be written in terms of the ion energy distribution $F(E_i)$, through the transformation

$$F(E_i) = f(u_i)\frac{\mathrm{d}u_i}{\mathrm{d}E_i} = \frac{f\left(\sqrt{2E_i/m_i}\right)}{\sqrt{2m_iE_i}} \tag{8}$$

Define E_p as the maximum of the energy distribution function, or equivalently the most-probable energy, such that

$$\left.\frac{\mathrm{d}F}{\mathrm{d}E_i}\right|_{E_i = E_p} = 0 \tag{9}$$

It is possible to relate the equivalent ion drift velocity to the most-probable energy as

$$u_d = \sqrt{2E_p/m_i} + (1/2\beta)\sqrt{m_i/2E_p} \tag{10}$$

Thus, the correct drifting Maxwellian energy distribution is computed from Eq. (7) as

$$F(E_i) = \sqrt{\frac{\beta}{2\pi m_iE_i}}\exp\left[-\beta\left(\sqrt{\frac{2E_i}{m_i}} - \sqrt{\frac{2E_p}{m_i}} - \frac{1}{2\beta}\sqrt{\frac{m_i}{2E_p}}\right)\right] \tag{11}$$

Now, define E_{-1} as one of the two energy values where $F(E_i)$ falls by a factor of e^{-1} from its peak, namely, $F(E_{-1}) = e^{-1}F(E_p)$. The equation

$$e^{-1} = \sqrt{\frac{E_p}{E_{-1}}}\exp\left\{-\beta\left[\left(\sqrt{\frac{2E_{-1}}{m_i}} - \sqrt{\frac{2E_p}{m_i}} - \frac{1}{2\beta}\sqrt{\frac{m_i}{2E_p}}\right)^2 - \left(\frac{1}{2\beta}\sqrt{\frac{m_i}{2E_p}}\right)^2\right]\right\} \tag{12}$$

can be solved for β, and, hence T_i, with the result that

$$\frac{kT_i}{E_p} = \frac{(\varepsilon - 1)^2}{\varepsilon - \ell n\varepsilon} \tag{13}$$

where $\varepsilon \equiv \sqrt{(E_{-1}/E_p)}$.

With the preceding analysis, the measured total ion voltage distribution displayed in the top of Fig. 8 can be analyzed to yield measurements of the equivalent ion temperature, under the simplifying approximation that the flow is entirely Xe^{+}, so that $q = 1$ and $E_i = eV_i$,

$$T_{\mathrm{eV}} = \frac{kT_i}{e} = \frac{(\varepsilon - 1)^2}{\varepsilon - \ell n\varepsilon}V_p \tag{14}$$

where T_{eV} is the ion temperature expressed in electron volts and V_p is the most-probable ion voltage. From the data of Fig. 8, $V_p = 267$ V, whereas $V_{-1} = 295$ and 237 (V_{-1} is the value of voltage where the distribution falls by a factor of e^{-1} from its value at V_p). By use of Eq. (14), two values of ion temperature are computed as 0.69 and 0.90 eV, dependent on which of the two V_{-1} points are used. Although not apparent from a cursory inspection of the MBMS data, proper analysis shows these results to be in excellent agreement with the value of $T_{eV} = 0.7$ eV obtained by Manzella.[7]

VI. Conclusions

The MBMS provided a direct measurement of the ionization fraction of the propellant within the SPT-100 plume independent of a model describing the plasma equilibrium state. These values compared very well with the same quantities measured previously using an emission spectroscopic techinque. Thus, it can be confidently assumed that the plume plasma in the SPT-100, when operating nominally at 300 V, 5 mg/s, is composed of 89% Xe^+, 11% Xe^{2+}, and less than 1% Xe^{3+}, with a heavy-particle distribution temperature between 0.69 and 0.90 eV.

In addition to an analysis of the majority propellant ions, the MBMS confirmed the existence of entrained background gasses caused by vacuum facility imperfections. These gasses were evidenced by the appearance of nitrogen, oxygen, and water vapor within the high-energy plasma mass species. Ground-test facility interactions were also manifested by the appearance of carbon ions within the plume caused by sputtering of protective graphite used in the proximity of the thruster.

Acknowledgments

This research benefited from the generous support of the Air Force Office of Scientific Research represented by M. Birkan, NASA John H. Glenn Research Center at Lewis Field, with equipment Grants administered by J. Sankovic, and support from NASA Johnson Space Center under the direction of R. Barton. The unique opportunity to evaluate a state-of-the-art thruster was made available by a generous equipment loan from M. Day of Space Systems/Loral. This support is gratefully acknowledged. Additionally, the authors would like to thank technicians W. Eaton, T. Larrow, G. Gould, T. Griffin, and D. McLean for assitance with hardware fabrication. The first author would also like to thank the research staff of the Plasmadynamics and Electric Propulsion Laboratory, namely, M. Domonkos, C. Marrese, F. Gulczinski, J. Haas, S. Kim, and G. Williams for their discussions in the preparation of this manuscript.

References

[1] King, L., "Transport Properties and Mass Spectral Measurements in the Plasma Exhaust Plume of a Hall-Effect Space Propulsion System," Ph.D. Dissertation, Dept. of Aerospace Engineering, Univ. of Michigan, Ann Arbor, MI, May 1998; also Univ. Microfilm International, Ann Arbor, MI, 1998.

[2] Bugrova, A., Desyatskov, A., and Kharchevnikov, V., "Experimental Determination of Ion Energy at the Outlet of SPT-ATON," *24th International Electric Propulsion Conference*, IEPC Paper 95-47, Electric Rocket Propulsion Society Press, 1995.

[3] King, L. B., Gallimore, A. D., and Marrese, C. M., "Transport-Property Measurements in the Plume of an SPT-100 Hall-Effect Thruster," *Journal of Propulsion and Power*, Vol. 14, No. 3, 1998, pp. 327–335.

[4] Myers, R., and Manzella, D., "Stationary Plasma Thruster Plume Characteristics," *Proceedings of the 23rd International Electric Propulsion Conference*, IEPC Paper 93-096, Electric Rocket Propulsion Society Press, Sept. 1993.

[5] Absalamov, S., Andreev, V., Colbert, T., Day, M., Egorov, V., Gnizdor, R., Kaufman, H., Kim, V., Korakin, A., Kozubsky, K., Kudravzev, S., Lebedev, U., Popov, G., and Zhurin, V., "Measurement of Plasma Parameters in the Stationary Plasma Thruster (SPT-100) Plume and Its Effect on Spacecraft Components," AIAA Paper 92-3156, July 1992.

[6] Marrese, C., Majumdar, N., Haas, J., Williams, G., King, L., and Gallimore, A., "Development of a Single-Orifice Retarding Potential Analyzer for Hall Thruster Plume Characterization," *Proceedings of the 25th International Electric Propulsion Conference*, IEPC Paper 97-066, Aug. 1997.

[7] Manzella, D., "Stationary Plasma Thruster Plume Emissions," *Proceedings of the 23rd International Electric Propulsion Conference*, IEPC Paper 93-097, Electric Rocket Propulsion Society Press, Sept. 1993.

[8] King, L. B., and Gallimore, A. D., "Ion Energy Diagnostics in the Plasma Exhaust Plume of a Hall Thruster," *Journal of Propulsion and Power*, Vol. 16, No. 5, 2000, pp. 916–922.

[9] Pollard, J., "Plume Angular, Energy, and Mass Spectral Measurements with the T5 Ion Engine," AIAA Paper 95-2920, July 1995.

[10] Gallimore, A. D., Kim, S. W., Foster, J. E., King, L. B., and Gulczinski, F. S., "Near- and Far-Field Plume Studies of a One-Kilowatt Arcjet," *Journal of Propulsion and Power*, Vol. 12, No. 6, 1996, pp. 105–111.

[11] Hutchinson, I. H., *Principles of Plasma Diagnostics*, Cambridge Univ. Press, Cambridge, England, U.K., 1987, Chap. 3.

[12] Bishaev, A., and Kim, V., "Local Plasma Properties in a Hall-Current Accelerator with an Extended Acceleration Zone," *Soviet Physics—Technical Physics*, Vol. 23, Sept. 1978, pp. 1055–1057.

[13] Baranov, V., Nazarenko, Y., Petrosov, V., Vasin, A., and Yashnov, Y., "Energy Model and Mechanisms of Acceleration Layer Formation for Hall Thrusters," AIAA Paper 97-3047, July 1997.

[14] Lide, D. R. (ed.), Handbook of Chemistry and Physics, 75th ed., CRC Press, Boca Raton, FL, 1994, p. 10-206.

[15] King, L. B., and Gallimore, A. D., "Identifying Charge-Exchange Collision Products Within the Ion-Energy Distribution of Electrostatically Accelerated Plasmas," *Physics of Plasmas*, Vol. 6, No. 7, 1999, pp. 2936–2942.